Journal of Information Hiding and Multimedia Signal Processing ©2019 ISSN 2073-4212
Ubiquitous International Volume **10**, Number **1**, January **2019**

Image Fusion Adopting Guided Filter and Multi-resolution Singular Value Decomposition

Peng Geng

School of Information Science and Technology
Shijiazhuang Tiedao University
No.17, Beierhuan East Road,Shijiazhuang, 050000, China
Gengpeng@stdu.edu.cn

Zhaoyang Wang

School of Information Science and Technology
Shijiazhuang Tiedao University
No.17, Beierhuan East Road, Shijiazhuang, 050000, China

Xiuming Sun*

Zhangjiakou University
No. 19, Pingmen Road, Qiaoxi District, Zhangjiakou,075000, China
*Corresponding author: 19279843@QQ.com

Received August 2016; Revised August 2018

Abstract. *A fast and effective image fusion method is proposed for creating a highly informative fused image through merging multiple source images. Firstly, the source images are decomposed into approximation component and detail component by multi-resolution singular decomposition. Secondly, the tenengrad function and modified spatial frequency are calculated as the contrast metric of the approximation and detail component, respectively. Thirdly, the guided filter is guided by the tenengrad function and modified spatial frequency when approximation and detail component are used as the input image, respectively. Finally, the output images of the guided filter are adopted to generate the decision map to merge the source images. Experimental results demonstrate that the proposed method can obtain state-of-the-art performance in merging of multi-focus and multimodal medical images.*
Keywords: Image fusion, Guided filter, Spatial frequency, Multi-resolution SVD, Tenengrad

1. **Introduction.** Image fusion plays an important role in various images processing such as feature extraction and target recognition. By the means of image fusion, different images with complementary information can be merged into a single fused image [1]. The fused image can provide more comprehensive information which is more useful for human and machine perception. A better image fusion method can not only preserve most of the important information of different images, but also produce little of artifacts in the fusion processing. Generally, image fusion methods can be separated into two groups such as spatial-based methods and transform-based methods. Spatial-based methods [2] include averaging and principal component analysis (PCA) [3] etc. Whereas the latter include the wavelets, contourlet transform [4], nonsubsampled contourlet transform (NSCT) [5], and shearlet transform [6]. Discrete wavelet transform would provide directional information

in decomposition levels and contain unique information at different resolutions. However, discrete wavelet transform is less effective in expressing the sharp transitions such as image edges and curve singularities due to its limitation of direction. The redundant decomposition in NSCT and shearlet causes the increase in computation complexity in the image fusion processing. Singular value decomposition(SVD) can convert the redundant image information in spatial domain into a few of singular values. Therefore, SVD-based fusion method has been used in many papers [7-10]. A video fusion algorithm [7] is presented based on the 3D surfacelet transform and the higher order singular value decomposition. Singular value decomposition is adopted to fuse the Quickbird panchromatic and multi-spectral data [8]. There is no the multi-resolution characteristic like wavelet transform in the these traditional SVD. Therefore, the idea of multi-resolution can be introduced into the SVD to construct the multi-resolution singular value decomposition (MSVD). On the other side, the fusion rule is vital to fused image quality. Recently, edge-preserving smoothing filters such as guided filter [11], weighted least squares [12] and bilateral filter [13] have been proposed in the area of image processing. The guided filter is edge-preserving filter avoid ringing artifacts and decreasing the decomposition computing time according to the independence of the filter size. The guided filter can be used in image enhancement, image smoothing, and image denoising etc. According to the guided filter's ability of enhancing image edge, we introduce guided filter into fusing the multi-resolution singular value decomposition components of source images. The presented method outperforms other fusion methods such as the max and average fusion rule based on MSVD, nonsubsampled contourlet transform, and cross bilateral filter.

2. **Guided Filter.** Guided filter is a type of edge-preserving smoothing operator, which filters the input image under the guidance of another image [14-15]. The guided filtering algorithm including the guiding image I, the input image p and an output image q. Theoretically, the guided filtering assumes a linear relationship between the input image and the output image in the local window centered at pixel k. The output image q can be expressed as:

$$q_i = a_k I_i + b_k, \qquad \forall_i \in \omega_i \tag{1}$$

Where a_k and b_k are constant in the window ω_i, respectively. The r decides the size of the window. The cost function of minimizing the difference between the output filtering q and input filtering p is shown following.

$$E\left(a_k, b_k\right) = \sum_{i \in \omega_k} \left(\left(a_k I_i + b_k - p_i\right)^2 + \varepsilon a_k^2\right) \tag{2}$$

In this equation, ϵ is a regularizer parameter to avoid a_k to be too big. The equation (2) can be calculated through linear regression adopting the following two equations [16]:

$$a_i = \frac{\frac{1}{|\varepsilon|}\sum_{i \in \omega_k}\left(I_i p_i - \mu_k \bar{p}_k\right)}{\sigma_k^2 + \varepsilon} \tag{3}$$

$$b_k = \bar{p}_k - a_k \mu_k \tag{4}$$

Where σ_k^2 and μ_k denote the variance and mean of ω_k in I , respectively. $|\epsilon|$ represents the number of pixels in ω_k. $\bar{p}_k$ is the mean of ω_k. The final filtering output is given by:

$$q_i = \frac{1}{\omega}\sum_{i \in \omega_k}\left(a_k I_i + b_k\right) = \bar{a}_k I_i + \bar{b}_k \tag{5}$$

3. **Multi-resolution Singular Value Decomposition.** For an arbitrary image matrix $A \in R^{m\times n}$, there is the orthogonal matrix $U \in R^{m\times n}$ which satisfied [17-18]:

$$U^T AV = \sum := \begin{bmatrix} \sum_1 & 0 \\ 0 & 0 \end{bmatrix} \tag{6}$$

Therefore, the A can be expressed as $A = U \sum V^T$. Where $\sum_1$ is a non-singular diagonal matrix size of $m \times n$. The diagonal elements of $\sum_1$ can be decreasingly aligned into the following.

$$\sigma_1 \geq \sigma_2 \geq ... \geq \sigma_r \geq 0 \tag{7}$$

Where r is the rank of matrix A. According to orthogonal matrix U and V depending on matrix A, the SVD is nonlinear. The A is equivalent to $\sum_1$, according to

$$A^T A = \begin{bmatrix} \sigma_1^2 & & & \\ & \sigma_2^2 & & \\ & & ... & \\ & & & \sigma_n^2 \end{bmatrix} \tag{8}$$

The larger singular value in the diagonal matrix above can be regarded as the approximation component of the image information. In a similar way, the smaller singular value can represent the detail component of the image. The $M \times N$ image I can be divided into non-overlapping 2×2 blocks and arrange each block into a 4×1 vector by stacking columns to form the data matrix X_1 . Decompose the data matrix I_1 by SVD, we can get $T = USV^T$, where U and V are orthogonal matrices with size of 4×4. T is multiplied by the U^T, we can get the matrix $A = U^T T = SV^T$. The elements in each row of A may be rearranged to form M/2×N/2 matrix A_1, A_2, A_3 and A_4. A_1 represents the approximation component the image I. And the A_2, A_3 and A_4 denote as the three detail components of the image I, respectively. The A_1, A_2, A_3 and A_4 are similar to the LL, LH, HL, and HH components of the traditional wavelet transform. Successively, next level of MSVD can be applied in the approximation component [19].

4. **Fusion Rule.**

4.1. **Fusion Rule of Approximation Component.** In the tenengrad function, the Sobel operator [20, 21] is adopted to calculate the spatial gradient in the vertical and horizontal directions of image. Tenengrad function can be given by the following formula [22]:

$$T(i,j) = \sum_i \sum_j \left[f_h^2(i,j) + [f_v^2(i,j)] \right] \tag{9}$$

Where $f_h(i,j)$ and $f_v(i,j)$ are the gradients along the horizontal and vertical direction, separately. They can be expressed as:

$$\begin{aligned} f_h(i,j) =& (f(i+1,j-1) + 2f(i+1,j) + f(i+1,j+1)) \\ & - (f(i-1,j-1) + 2f(i-1,j) + f(i+1,j+1)) \end{aligned} \tag{10}$$

$$\begin{aligned} f_v(i,j) =& (f(i-1,j+1) + 2f(i,j+1) + f(i+1,j+1)) \\ & - (f(i-1,j-1) + 2f(i,j-1) + f(i+1,j-1)) \end{aligned} \tag{11}$$

Owing to the guided filters ability to enhance the image detail part and image edge, the guided filter can be used as contrast performance metrics function of the image to more effectively extract the salience regions. When the tenengrad value of $MSVD^l(i,j)$

approximation component is adopted as the guide image in the guided filter, the output of the guided filter can be expressed as:

$$q^l(i,j) = \frac{1}{\omega}\sum_{k\in\omega_k}\left(a_k T^l(i,j) + b_k\right) = \bar{a}_k T^l(i,j) + \bar{b}_k \tag{12}$$

Where the parameter l denotes $q^l(i,j)$ and $T^l(i,j)$ that are calculated by the approximation component of the MSVD coefficient instead of the detail component. The contrast performance metrics of tenengrad function will be enhanced by the guided filter method guided by the tenengrad function of the MSVD approximation coefficients. So, the fusion decision map can be calculated as following.

$$Map^l(i,j) = \begin{cases} 1, & \text{if } q_A^l(i,j) \geq q_B^l(i,j)) \\ 0, & \text{if } q_A^l(i,j) < q_B^l(i,j)) \end{cases} \tag{13}$$

Thus, the new fused approximation component can be selected according to the decision map.

$$MSVD_F^l(i,j) = \begin{cases} MSVD_A^l(i,j), & \text{if } Map^l(i,j) \geq 1 \\ MSVD_B^l(i,j), & \text{if } Map^l(i,j) < 0 \end{cases} \tag{14}$$

Where $\text{MSVD}_A^l(i,j)$ are $\text{MSVD}_B^l(i,j)$ the MSVD approximation component of the source image A and B in MSVD domain. The A, B and F represent the source image A, source image B, and fused image F, respectively.

4.2. **Fusion Rule of Detail Component.** Spatial frequency (SF) [23-24] is calculated according to the row and column frequency of the image. The spatial frequency can be calculated according to the Eq. (15).

$$SF(i,j) = \sqrt{\frac{1}{MN}\sum_{i=1}^{M}\sum_{j=1}^{N}\left(I_{i,j} - I_{i,j-1}\right)^2 + \left(I_{i,j} - I_{i-1,j}\right)^2} \tag{15}$$

Where $I_{i,j}$ is the pixel value of the image in the i column and j row in the image I of M column and N row. However, the SF of the image is not enough to express the salience character due to lack of the direction information carried in the image. The modified spatial frequency [25] is capable of capturing the fine details carried in the image because of incorporating the direction information except for the row and column frequency. The modified spatial frequency can be calculated as:

$$MSF(i,j) = \sqrt{SF^2(i,j) + DF^2(i,j)} \tag{16}$$

Where $DF(i,j)$ is the direction frequency of the image.

$$DF(i,j) = \sqrt{\frac{1}{MN}\sum_{i=1}^{M}\sum_{j=1}^{N}\left(I_{i,j} - I_{i-1,j-1}\right)^2 + \left(I_{i-1,j} - I_{i,j-1}\right)^2} \tag{17}$$

The MSF of the source image can express the performance of contrast measure in the source image. Similarly, the MSF can be applied in transform domain to distinguish the contrast and clarity of multi-scale transform coefficients. Furthermore, the contrast performance metrics of MSF can be enhanced by guided filter method guided by modified spatial frequency of the MSVD detail component. Hence, the of $\text{MSD}^d(i,)j$the MSVD

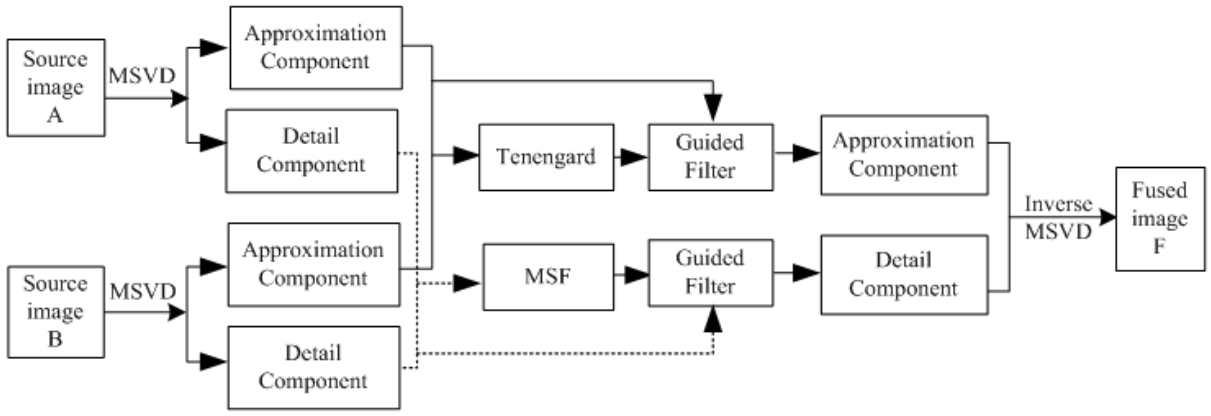

FIGURE 1. Schematic diagram of the proposed fusion method.

detail component is adopted as the guide image in the guided filter. The output of the guided filter can be expressed as:

$$q^h(i,j) = \frac{1}{\omega}\sum_{i\in\omega_k}(a_k MSF^h(i,j) + b_k) = \bar{a}_k MSF^h(i,j) + \bar{b}_k \tag{18}$$

Where the parameter h denotes that the $q^h(i,j)$ are $MSF^h(i,j)$ calculated by the detail component of the MSVD coefficient instead of the approximation component. Therefore, the fusion decision map can be illustrated as follows.

$$Map^h(i,j) = \begin{cases} 1, & \text{if } MSF_A^h(i,j) \geq MSF_B^h(i,j)) \\ 0, & \text{if } MSF_A^h(i,j) < MSF_B^h(i,j)) \end{cases} \tag{19}$$

Thus, the new fused detail component $MSVD^h(i,j)$ can be selected according to the following.

$$MSVD_F^h(i,j) = \begin{cases} MSVD_A^h(i,j), & \text{if } Map^h(i,j) = 1 \\ MSVD_B^h(i,j), & \text{if } Map^h(i,j) = 0 \end{cases} \tag{20}$$

The proposed approach is shown in Fig.1.

5. **Experiments and Discussion.** To demonstrate the effectiveness of the presented scheme, two groups of experiments have been executed. The first group of experiments are performed on multi-focus images shown in Fig.2(a)-(h). The second group of experiments are implemented on multimodal medical images shown in Fig.3 (a)-(d). Fig.3(a) and Fig.3(b) are the magnetic resonance imaging (MRI) and computed tomography (CT), respectively. Fig.3(c) and Fig.3(d) are the MRI and magnetic resonance angiography (MRA), separately. In the two groups of experiment, the performance of the proposed method is compared with those of the traditional MSVD method [10], the multi-scale geometry analysis method based on NSCT [25] and the cross bilateral filter method [26]. The Naidu's method based on the MSVD adopted the average and max rules to fuse the approximation component and the detail component, respectively. In the Sudeb's method based on NSCT, the source images are decomposed by the three scales. The directions in three scales are set to 1, 2, and 4, respectively. The 'pyrex' and 'vk' are utilized as the pyramid filter and orientation filter, respectively. The parameter shown in the paper [26] are adopted in the Kumar's method based on the cross bilateral filter. In the proposed method, the one level decomposition same as the Naidu's method is used in the MSVD. To show the effeteness of different local window radius Eps and regularization parameter r in guided filter, an experiments are conducted on Fig.3 (c) and Fig.3 (d) by proposed

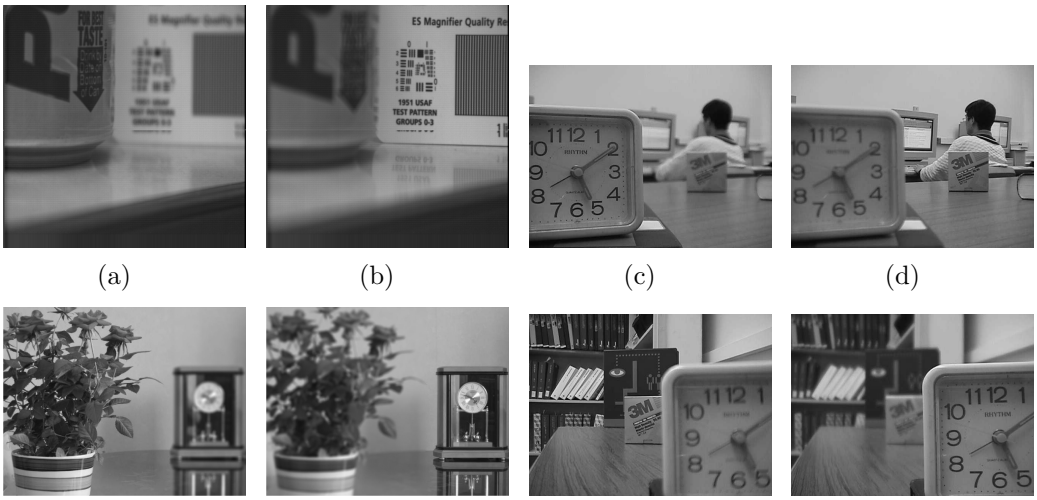

(a) (b) (c) (d)

(e) (f) (g) (h)

FIGURE 2. Source multi-focus images for fusion experiments. (a), (c), (e) and (g) focus on the left part; (b), (d), (f) and (h) focus on the right part.

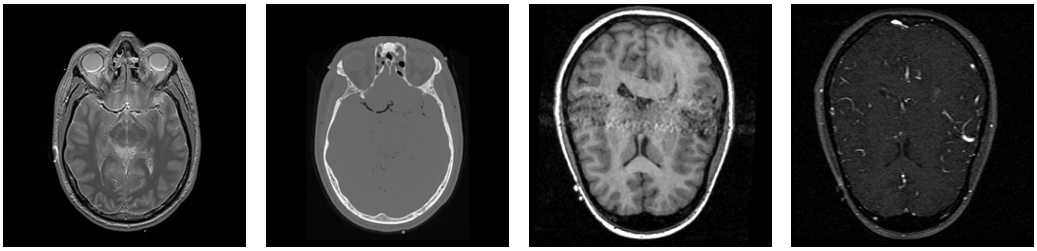

(a) (b) (c) (d)

FIGURE 3. Source multimodal images for fusion experiments. (a), CT; (b), MRI; (c) MRI; (d) MRA

method. The $Q^{AB/F}$ value by different parameters are shown in Tab.1. The right part of Tab.1 is the different $Q^{AB/F}$ values by different regularization value and the local window radius is set to 16. The right part of Tab.1 are different $Q^{AB/F}$ values by different local window radius value and regularization parameter is set to 0.04. There is not obvious difference by using different local window radius value and regularization. When local window radius is equal to 16 and regularization parameter is equal to 0.04, $Q^{AB/F}$ value is biggest. Hence, In this paper, the local window radius and regularization parameter of guided filter are set to 16 and 0.04, separately.

5.1. **Comparison on multi-focus image fusion.** Four pairs of multi-focus images shown in Fig.2 are utilized to evaluate the performance of the proposed scheme. Fig.4 demonstrates the fusion result by the proposed method and the other three methods mentioned above. For the sake of demonstrating the difference of fusion result, the enlarged part images of Fig.4 are illustrated in Fig.5. As shown in Fig.5(b), Naidu's method produces obvious blurred edges around the character. There are obvious artifacts in Fig.5(c) fused by Sudeb's method. Fig.5(d) shows better fusion result but introduces artifacts around character in the upper right section of Fig.5(d). There are minimal artifacts around the object boundaries images in Fig.5(a) fused by the proposed scheme. Furthermore, the enlarged part of the image demonstrate that there are more clear artifacts in

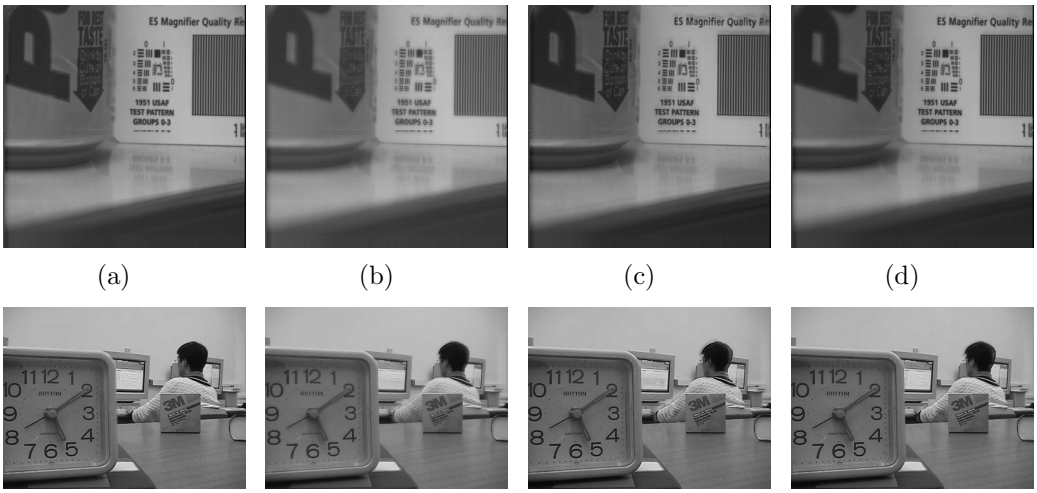

(a) (b) (c) (d)

(e) (f) (g) (h)

FIGURE 4. Source multi-focus images for fusion experiments.

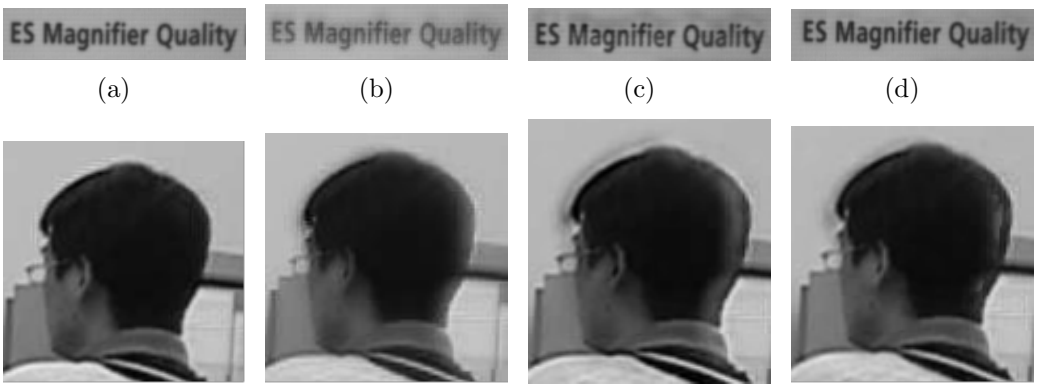

(a) (b) (c) (d)

(e) (f) (g) (h)

FIGURE 5. Comparisons on the enlarged part in Fig. 4.

Fig.5(g) and (h) than in Fig.5(f) and (e). Fig.5(e) shows the better image clarity and smaller artifact than the Fig.5(f) does. For comparison purpose, the $Q^{AB/F}$ metric [27] and mutual information (MI) [25] are employed as objective criteria. $Q^{AB/F}$ measures the amount of edge information transferred from the source images to the fusion images and MI computes how much information from source images is converted into the fusion result. The explanations of $Q^{AB/F}$ and MI metric are elaborately introduced in reference [27] and [25], respectively. It can be known that the larger of the objective criteria values and the clear fused image we get, the better fusion performance the method has. It can be obviously concluded from Tab.2 that all of the $Q^{AB/F}$ and MI value of four pair of multi-focus images fused by the proposed algorithms are largest in the four methods except the $Q^{AB/F}$ of Fig.4(d) produced by Kumar's method. However, the visual performance of above demonstrate that the Fig.4(e) by the proposed algorithms is obvious better than the Fig.4(d) by Kumar's method is. As a whole, the proposed scheme is effective in merging multi-focus images than the other three methods from both visual performance and the objective metrics.

5.2. **Comparison on multimodal medical image fusion.** Multimodal medical image fusion plays an import role in the clinic diagnosis and provides the physician with the

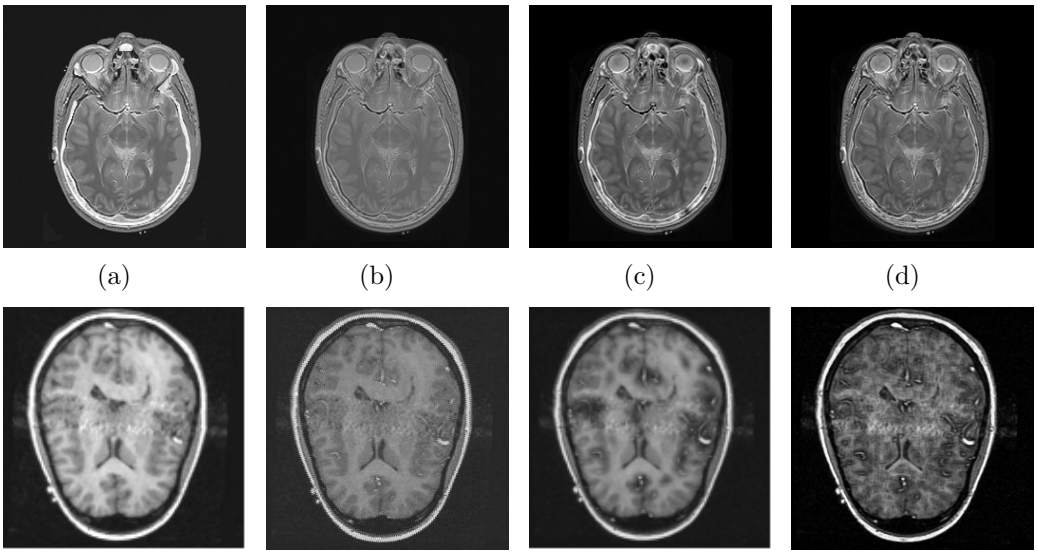

FIGURE 6. Source multimodal images for fusion experiments.

complementary image information merged by different modal image. The experiments on two pairs of multimodal medical images are executed to illustrate the effectiveness of the proposed method. The fused results produced by the four methods are demonstrated in the Fig.6. Obviously, Fig.6(b) lost all of white boundary in Fig.4 (b). The upper part of white boundary in Fig.4 (b) is lost in Fig.6(d). The labeled parts with white information transmitted from Fig.4 (b) are clearer than the corresponding part in Fig.6(d). From Fig.6(e)-(h), it is obvious that Fig.6(e) shows the higher clarity and contrast than the other three images does. There are many unwanted degradations in Fig.6(g) and Fig.6(h). From Tab. 3, $Q^{AB/F}$ and MI value of two pairs of multimodal medical images are largest in the four methods. Taken together, the proposed scheme is more effective than the other three methods from both visual performance and the objective metrics in merging the multimodal medical images.

5.3. **Computation time analysis.** Tab.4 demonstrates the computation time of all methods. Kumar's method is the slowest and Naidu's method is the fastest. The proposed method is faster than Sudeb's method and Kumar's method. Because the modified spatial frequency and the guided filter need 80 percent time to produce the decision map. It spends about 70 percent time on the firing times of the PCNN about seventeen direction subbands by the NSCT decomposition in the Sudeb's method the PCNN. In the whole, the proposed method is better in the fusion image quality than the Kumar's method and Naidu's method with effectively reducing time complexity.

6. **Conclusion.** A fast and effective image fusion method adopting guided filtering is proposed to fuse the multi-focus images and multi-modal medical images. The proposed algorithm utilizes multi-resolution singular value decomposition to decompose the source images into approximation component and detail component like the traditional wavelet. The tenengrad function and the modified spatial frequency are adopted to evaluate the contrast and clarity of the approximation component and detail component, respectively. More importantly, the guided filter has the nice edge-preserving smoothing property when it is used to enhance the different contrast performance functions. The output of the

guided filter guided by tenengrad function and modified spatial frequency is used to create the accurate and effective decision map. Experiments demonstrate that the proposed method can well preserve the original and complementary information of source images. Furthermore, the proposed method is computationally efficient in comparison with different methods in the computation time.

TABLE 1. Different $Q^{AB/F}$ by different parameters.

Eps	$Q^{AB/F}$	r	$Q^{AB/F}$
Eps=0.01	0.7211	r=1	0.7129
Eps=0.04	0.7375	r=4	0.7183
Eps=0.08	0.7358	r=8	0.7218
Eps=0.16	0.7321	r=12	0.7219
Eps=0.20	0.7255	r=16	0.7375
Eps=0.24	0.723	r=20	0.7243
Eps=0.28	0.7218	r=24	0.7139

TABLE 2. Objective evaluation on the multi-focus images fusion result.

Images	Metric	Proposed	Naidu's	Sudeb's	Kumar's
Pepsi	MI	**8.0900**	6.5321	7.6071	7.8872
	$Q^{AB/F}$	0.7770	0.6709	0.7567	**0.8628**
Lab	MI	**7.7038**	6.9411	7.7021	7.4774
	$Q^{AB/F}$	**0.7375**	0.6221	0.7178	0.7321
Bonsai	MI	**8.1741**	6.0158	7.0524	6.8310
	$Q^{AB/F}$	**0.7288**	0.5668	0.6868	0.6923
Disk	MI	**8.0220**	5.8289	7.0584	6.6735
	$Q^{AB/F}$	**0.7248**	0.5587	0.6978	0.6950

TABLE 3. Objective evaluation on the multimodal images fusion result.

Images	Metric	Proposed	Naidu's	Sudeb's	Kumar's
MRI and CT	MI	**4.6448**	3.6832	4.0060	4.3780
	$Q^{AB/F}$	**0.6262**	0.4656	0.6042	0.6164
MRI and MRI	MI	**4.0902**	3.5877	3.8245	3.7450
	$Q^{AB/F}$	**0.5442**	0.4247	0.5823	0.5364

Acknowledgment. This work was supported in part by National Natural Science Foundation of China under grants 61702347, 61401308 and 61572063, the Natural Science Foundation of Hebei Province under grants F2018210148, F2016201142, F2016201187 and F2017210161, and Education Department of Hebei Province under grant QN2017132. The authors also thank the anonymous referees for their valuable suggestions.

TABLE 4. Computation time for different methods (unit: second).

Images	Size	Proposed	Naidu's	Sudeb's	Kumar's
Fig.3(a)-(b)	464 × 464	**4.6448**	3.6832	4.0060	4.3780
		0.6262	0.4656	0.6042	0.6164
Fig.3(c)-(d)	256 × 256	**4.0902**	3.5877	3.8245	3.7450
		0.5442	0.4247	0.5823	0.5364
Pepsi	512 × 512	**4.6448**	3.6832	4.0060	4.3780
		0.6262	0.4656	0.6042	0.6164
Disk	480 × 640	**4.6448**	3.6832	4.0060	4.3780
		0.6262	0.4656	0.6042	0.6164
Bonsai	944 × 736	**4.6448**	3.6832	4.0060	4.3780
		0.6262	0.4656	0.6042	0.6164

REFERENCES

[1] S. T. Li, X. D. Kang, and J. W. Hu, Image Fusion with Guided Filtering, *IEEE Transactions on Image Processing*, vol. 22, no.7, pp. 2864–2875, 2013.

[2] Y. Ma, J. Chen, C. Chen, F. Fan, J. Y. Ma, Infrared and visible image fusion using total variation model , *Neurocomputing*, vol. 202, pp.12–19, 2016.

[3] Y.X. Zhang, C. Li, Z. H. Zhao, J. Jia and J. Liu, Multi-focus image fusion based on robust principal component analysis and pulse-coupled neural network, *Optik*, vol.125, no. 17, pp. 5002–5006, 2014.

[4] M. N. Do, V. Martin, The contourlet transform: An efficient directional multiresolution image representation, *IEEE Transactions on Image Processing*, vol. 14, no. 12, pp. 2091–2106, 2005.

[5] L. L. Li, Y. J. Si, Z. H. Jia, A novel brain image enhancement method based on nonsubsampled contourlet transform, *International Journal of Imaging Systems and Technology*,vol. 28, no. 2, pp. 124–131, 2017.

[6] K. Meshkini, H. Ghassemian, Texture classification using Shearlet transform and GLCM *2017 Iranian Conference on Electrical Engineering (ICEE)* , pp. 1845–1850, 2017.

[7] Q. Zhang, Y. B. Wang, L. Martin, X. Q. Yuan and L. Wang, Multisensor video fusion based on higher order singular value decomposition, *Information Fusion*, vol. 24, no.C, pp. 54–71, 2015.

[8] S. Koduri, Multisensor data fusion with singular value decomposition, *14th International Conference on Modelling and Simulation*, pp. 422–426, 2012.

[9] L. Jing, F. H. Liu, A novel image fusion approach combined singular value decomposition with averaging operation, *Lecture Notes in Electrical Engineering*, 208, pp. 789–794, 2013.

[10] V. P. S. Naidu, Image Fusion technique using Multi-resolution singular Value decomposition, *Defence Science Journal*, vol. 61, no. 5, pp. 479–484, 2011.

[11] K. M. He, J. Sun, X. O. Tang, Guided image filtering, *11th European Conference on Computer Vision*, pp. 1–4, 2010.

[12] J. Jaehoon, Use of weighted least squares for geo-positioning using dual-satellite image pairs, *International Journal of Remote Sensing*, vol. 38, no. 6, pp. 1682–1701, 2017.

[13] A. A. Saime, Determination of optimal parameters for bilateral filter in brain MR image denoising, *Applied Soft Computing*, vol.43, no. C, pp. 87–96, 2016.

[14] Manhood, M. Tariq, MRT Letter: Guided filtering of image focus volume for 3D shape recovery of microscopic objects, *Microscopy Research and Technique*, vol. 77, no. 12, pp. 959–963, 2014.

[15] D. P. Bavirisetti, V. Kollu, X, Gang and D. Ravindra, Fusion of MRI and CT images using guided image filter and image statistics, *International Journal of Imaging Systems and Technology*, vol. 27, no. 3, pp. 227–237, 2017.

[16] H. Pang, A. C. Oscar, Z. Guo Improved single image dehazing using guided filter, *Asia-Pacific Signal and Information Processing Association Annual Summit and Conference*, pp.522–525, 2011.

[17] M. Sunda, G. Mazzarella and M. Migliaccio, A numerical study on the SVD-based retrieval of radiometric data, *IEEE Antennas and Propagation Society, AP-S International Symposium (Digest)*, pp.732–735, 2001.

[18] N. M. Makbol,B. E. Khoo, A new robust and secure digital image watermarking scheme based on the integer wavelet transform and singular value decomposition, *Digital Signal Processing*, vol. 2014, no. 33, pp. 134–147, 2014.

[19] X. Z. Zhao, B. Y. Ye, Multi-resolution SVD packet theory and its application to signal processing, *Acta Electronica Sinica*, vol. 40, no. 10, pp. 2039–2046, 2012.

[20] X. Xu, Y. L. Wang, X. L. Zhang, S. X. Li, X. M. Liu, X. F. Wang and J. S. Tang, A comparison of contrast measurements in passive autofocus systems for low contrast images, *Multimedia Tools and Applications*, vol. 69, no. 1, pp. 139–156, 2014.

[21] K. Lee, P. S. Y. Lee, Object-based auto exposure and focus algorithms based on the human visual system, *IEICE Transactions on Fundamentals of Electronics, Communications and Computer Science*, vol. E92-A, no. 3, pp. 832–835, 2009.

[22] O. K. Kwon, S. G. Kong, Sharpness-enhancing enlargement of terahertz images, *IEEE Transactions on Electronics. Information and Systems*, vol. 133, no. 4, pp. 908–909, 2013.

[23] A. Eskicioglu, P. Fisher, Image quality measures and their performance, *IEEE Transaction on Wireless Communications*, vol. 43, no. 12, pp. 2959–2965, 1995.

[24] Y. Zheng, E. Essock, B. Hansen and A. Haun, New metric based on extended spatial frequency and its application to DWT based fusion algorithms, *Informaiton Fusion*, vol. 8, no. 2, pp. 177–192, 2007.

[25] D. Sudeb, K. M. Kumar, NSCT-based multimodal medical image fusion using pulse-coupled neural network and modified spatial frequency, *Medical and Biological Engineering and Computing*, vol. 50, no. 10, pp. 1105–1114, 2012.

[26] B. K. Shreyamsha Kuma, Image fusion based on pixel significance using cross bilateral filter, *Signal, Image and Video Processing*, vol. 9, no. 5, pp. 1193–1204, 2015.

[27] G. Piella, A general framework for multiresolution image fusion: from pixels to regions, *Information Fusion*, vol.4, no. 4, pp. 259–280, 2003.